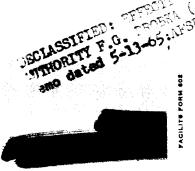# TECHNICAL MEMORANDUM
X-109

THE WIND-INDUCED LOADS ON A DYNAMICALLY SCALED MODEL

OF A LARGE MISSILE IN LAUNCHING POSITION

By Donald A. Buell and George C. Kenyon

Ames Research Center
Moffett Field, Calif.

N65-28202

(ACCESSION NUMBER)

_36_

(PAGES)

(NASA CR OR TMX OR AD NUMBER)

(THRU)

(CODE)

_01_

(CATEGORY)

NATIONAL AERONAUTICS AND SPACE ADMINISTRATION

WASHINGTON   December 1959

CONFIDENTIAL

NATIONAL AERONAUTICS AND SPACE ADMINISTRATION

TECHNICAL MEMORANDUM X-109

THE WIND-INDUCED LOADS ON A DYNAMICALLY SCALED MODEL

OF A LARGE MISSILE IN LAUNCHING POSITION*

By Donald A. Buell and George C. Kenyon

SUMMARY

Wind-tunnel tests were made of a model of a large missile in launching position. Ground winds were simulated at Reynolds numbers up to 7 million based on the maximum diameter of the model, and the dynamic response of the model was determined. Measurements were made of the bending moments, accelerations, and average drag of the model with and without various modifications. In addition, dynamic air pressures on the sides of the model were measured.

The results showed that wind may induce model motions which have a randomly varying amplitude and which can produce transverse loads much larger than the dragwise loads. However, certain small modifications to the model, particularly near the nose, greatly reduced the fluctuating loads.

INTRODUCTION

The action of wind on a missile in launching position induces stresses in the drag direction and also in a plane perpendicular to the wind direction. It is important to know the magnitude of these wind-induced loads not only for considerations of structural integrity, but also for proper guidance-system alinement and for prediction of drift of the missile at launch. The shape of large missiles in launching position resembles that of a smokestack, and the problem of wind-induced oscillations has long been recognized in smokestack design. Reference 1 is an example of a recent investigation into the problem.

Much data has been compiled in the past on the flow around circular cylinders, but it has been confined chiefly to subcritical Reynolds numbers (less than 500,000 approximately). At these Reynolds numbers,

*Title, Unclassified

the pressure fluctuations on the cylinder have a predominant frequency
associated with the familiar Kármán vortex street in the wake. For large
cylindrical missiles, however, the Reynolds numbers of interest are super-
critical. At these Reynolds numbers the boundary layer is turbulent as
it separates from the cylinder, and the pressures in the wake tend to
have a random fluctuation. The random oscillatory forces arising from
this type of flow have recently been measured on a two-dimensional model,
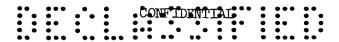and the results are reported in references 2 and 3.

Very little is known about the unsteady aerodynamic loads on three-
dimensional cylinders at large Reynolds numbers and the influence of the
structural dynamics of the cylinders on the aerodynamic loads. The lack
of information in this regard led to a wind-tunnel investigation of the
effects of winds on a dynamically scaled model of a ballistic missile in
the launch position. The wind tunnel and the scale of the model used for
the investigation were selected to provide full-scale Reynolds numbers
and reduced frequencies of the missile without introducing aerodynamic
compressibility effects. The tests were performed in the Ames 12-foot
pressure wind tunnel with a model having external dimensions 1/10 of
those of the actual missile. The model was designed and constructed by
The Martin Company of Denver, Colorado.

Measurements were made of the accelerations and strains induced in
various parts of the model by winds having equivalent full-scale veloc-
ities up to 80 miles per hour. The average forces and moments on the
model as a whole were also measured. The effects of external modifica-
tions near the nose, surface roughness, and presence of nearby structures
were investigated.

A-173

NOTATION

C_D drag coefficient, $\dfrac{drag}{qS}$

D diameter

f frequency of oscillation

g acceleration due to gravity

l length of cylindrical portion of second stage

m mass

p_t total pressure

Δp root mean square of the increment of pressure across the second
     stage

q   dynamic pressure

rms   root mean square

S   frontal area

V   velocity

ρ air density

APPARATUS

Model and Support

The model consisted of an aluminum structural shell with external dimensions 1/10 those of the full-scale Titan missile, and with enclosed weights and instrumentation as shown in figure 1. The stiffness and mass of the model evolved from the requirement that Reynolds number, frequency, and dynamic deflections of the missile be properly simulated. To obtain full-scale Reynolds numbers, the model wind speed was twice full-scale values and the air density was five times standard sea-level atmospheric density. Lead weights in the model were of such a size that the relative density factor $m/\rho D^3$ was the same for the model as for the missile, and the weights were positioned so as to approximate the mass distribution of the fully loaded missile. The structural shell was made of the same material as the missile with cross-section moments of inertia 0.002 of those of the missile. This stiffness and mass distribution gave the model a natural frequency 20 times the full-scale value and made the dimensionless frequency parameter fD/V (Strouhal number) the same for the model as for the missile. With this dynamic scaling and with structural damping of the missile equal to that of the model, the model deflections would be 1/10 of the full-scale deflections and the bending moments would be 1/50 of the simulated bending moments on the missile (ref. 2 discusses the effect of damping). Figure 2 shows the mass and stiffness characteristics of the model.

For measurements of the dynamic characteristics the model was bolted to a 4-inch-thick steel base which was in turn bolted to the tunnel shell. A steel fairing was provided over the base support.

For measurements of the steady drag and overturning moment the model was attached directly to the conventional lever-type balance system of the wind tunnel. A 4-foot-diameter plate attached to the model and flush with the tunnel floor prevented leakage near the model during the balance-system measurements. Some of the lead weights were removed from the model during the balance-system measurements to prevent allowable structural loads from being exceeded at large wind speeds.
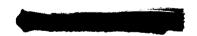
CONFIDENTIAL

Considerable effort was expended to eliminate relative motion at model and support joints during the oscillation measurements. This was greatly facilitated by shaking the model with an electromagnetic shaker, connected to the model as shown in figure 3. Model joints which showed relative motion were effectively tightened by applying adhesive between joint surfaces. The exterior surface of the model was filled, painted, and sanded smooth with number 400 sandpaper with the exception of the screw holes at the tip. These holes were filled and faired into the nose contour with wax.

Modifications and additions to the exterior of the model were numerous, particularly near the nose. In figure 4 are shown some of the revisions which will be discussed. The model was also tested in the presence of an "umbilical" tower which is shown in figure 5 in one of the four positions tested. The appearance of the model surface in figure 5 is not representative of the model as tested.

The wind tunnel in which the tests were performed has an air stream of exceptionally low turbulence by virtue of a large contraction ratio (25 to 1 in area) and the use of eight fine-mesh screens in the settling chamber. Hot-wire measurements of the longitudinal mass-flow fluctuation have indicated a root-mean-square amplitude of considerably less than 0.1 percent at the speeds of interest here. Hot-wire measurements during the tests showed that the model had no effect on the turbulence in front of the model.

Model Instrumentation

The model instrumentation consisted of strain gages bonded to the model shell at five stations, accelerometers in the tip and on the base support, and dynamic pressure transducers at one station. The strain gages were mounted four to a station and were wired in pairs to indicate bending in and perpendicular to the wind direction. Two linear accelerometers in the tip indicated movement in the transverse direction with two different sensitivities (5g and 50g maximum acceleration). A torsional accelerometer was mounted near the nose to show torsional movement about the longitudinal axis of the model (very little movement was detected, however). Two linear accelerometers on the base support were situated so as to indicate the horizontal and rotational movement of the base in the plane perpendicular to the wind. The pressure transducers were placed in the model near the middle of the simulated second-stage shell on a diameter normal to the air stream and were wired to indicate pressure difference across the model. A 3 kilocycle carrier frequency was used for the power supply of the strain gages and one tip accelerometer, and batteries supplied the other accelerometers. A 20 kilocycle current powered the pressure transducers. All output signals, properly

amplified, were recorded on an oscillograph, and in addition the signals from the pressure transducers, a tip accelerometer, and the strain gages at the base were recorded on magnetic tape.

The wind-off damping of the model was determined in the wind tunnel from the rate of decay of oscillations which were excited by one of two methods. One method was to deflect the tip of the model by means of a turnbuckle arrangement and then cut the restraining member. The result of this procedure was a predominantly first-mode oscillation and a small higher frequency oscillation which decayed more rapidly than the first. This method of excitation was applied in both the dragwise direction and the transverse direction. The second method of excitation was by means of the shaker previously referred to and gave a pure first-mode oscillation more nearly representative of the wind-induced motion. However, it was applied in the transverse direction only. The results of these measurements are shown in figure 6 and indicate that the measured damping was about 0.6 percent of critical in the transverse direction and probably half this amount in the dragwise direction. The measured natural frequency of the first-mode oscillations was about 15 cycles per second in the transverse direction and 16-1/2 cycles per second in the dragwise direction. The distribution of the bending moments induced by the shaker is shown in figure 2 and is essentially the same as any of the first-mode oscillations observed during the tests.

TESTS

The procedure for the dynamic tests was to subject the model to winds of various speeds and measure the amplitude of the fluctuating bending moments, acceleration, and pressures experienced by the model. The average dragwise bending moments were determined at the same time, but the accuracy was somewhat limited because of zero shifts and the high attenuation required to keep the oscillograph traces orderly and facilitate their identification. A more accurate determination of the average drag and overturning moment was obtained later with the model mounted on the tunnel balance system.

The oscillation tests were performed at a total pressure of 75 pounds per square inch absolute, and the average free-stream static density was 0.0113 slug per cubic foot. For each configuration the wind velocity was varied from 0 to about 160 miles per hour or to the velocity at which the stress limits of the model were reached. At the maximum velocity, the Reynolds number per foot was 7 million, and the Mach number was 0.2.

The static-drag tests were performed at the same Reynolds numbers and Mach numbers as were the dynamic tests. However, limits in velocity imposed as a result of excessive model oscillation during the dynamic tests were avoided for the static tests by removal of the internal weights
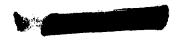
6

from the upper portion of the model. A few measurements of the drag were made at Reynolds numbers down to 70,000. In these tests the density was reduced in steps down to 0.0006 slug per cubic foot, and the Mach number was varied up to a maximum of 0.3.

DATA REDUCTION

Bending Moments

The output signal of the strain gages consisted of a fluctuating voltage which was related to the bending moment by factors that had been evaluated prior to the tests. Samples of the signals from gages at the base of the model are shown in figure 7 for a test velocity of 139 miles per hour. Signals from gages near the nose of the model had a larger high-frequency fluctuation imposed on the first-mode wave but were otherwise similar to those shown. The length of the entire data sample for each test velocity was generally between 30 seconds and 1 minute. Reduction of the data sample began with the selection of the maximum transverse bending moment, assumed to be half the maximum difference between adjacent peaks. Several values of the dragwise bending moment were recorded. One value was the maximum within one or two cycles of the point of maximum transverse bending moment. This point occasionally coincided with the point of maximum dragwise fluctuation, but there appeared to be no consistent relation between the two points. In addition, the maximum dragwise fluctuations in the data sample and the average dragwise bending moments were also recorded.

A correlation between the maximum transverse bending moment and the root-mean-square value of the transverse bending moment was desired because mathematical analyses of random processes are ordinarily in terms of root-mean-square values (c.f., ref. 2). To achieve this, the tape-recorded signals were passed through a thermocouple-type mean-square meter, and the mean-square output was recorded. The calibration of the recorder output in terms of bending moment was made by means of shaker-induced oscillations at constant amplitude recorded simultaneously on the oscillograph and tape. In an effort to produce a constant reading for wind-on tests, condensers were introduced into the circuit of the mean-square meter, increasing the time constant for its response to 7-1/2 seconds. The resulting output of this meter is shown in the lower part of figure 7. The rather large and erratic changes in value, despite the sluggish instrument response, are descriptive and typical of the model motion. Integration of the area under the curve was used to determine the mean squared bending moment for the complete data sample. The square root of this quantity provided the desired information for comparison with the previously determined maximum bending moment.

Accelerations

Accelerometer outputs were similar to the strain-gage outputs with the exception that higher frequencies than the first mode were also evident. The output of one of the accelerometers in the model nose was fed into a galvanometer which had a flat response curve up to only 30 cycles per second, and this procedure eliminated much of the "hash." Mean-squared values of acceleration had the same variations as those of bending moment. Tip deflections were computed from the tip accelerations and frequency on the assumption that the fluctuations were sinusoidal.

Pressure Fluctuations

The output of the pressure transducers consisted of a randomly fluctuating voltage which was related to pressure by means of a static pressure calibration. The tape-recorded signal was passed through a wave analyzer which determined the power spectral density of the data sample at frequencies from 5 to 100 cycles per second for a band width of 1-1/2 cycles per second. Some model configurations caused the amplitude of the pressure fluctuations to reach a peak at specific frequencies, but the concentration of energy was not at all large and rarely occurred at the natural frequency of the model. The pressure fluctuation amplitudes which will be presented are root-mean-square values taken from the frequency analyses at the natural frequency of the model.

Corrections

Corrections were applied to the measured dynamic pressure to account for the blockage of the model, of the umbilical tower, and of the wakes of the model and tower. The blockage corrections were computed by the method of reference 4 and increased the velocity by amounts up to 3 percent. A correction, also computed according to this reference, was applied to the drag measured in the static-force tests to account for the wake-induced pressure gradient in the air stream. This correction reduced the drag by less than 1 percent. In the static-force tests the presence of the model induced moment tares on the balance-system turntable which amounted to about 15 percent of the overturning moment at the base of the model. The turntable was a plate 4 feet in diameter at the base of the model, perpendicular to the model axis, and exposed to the air stream. The turntable tare was assumed to be the difference between the measured pitching moments and the average dragwise bending moments measured in the dynamic tests. Although the accuracy of the dynamic data was not comparable to that of the balance system, tests of

many configurations were available with which to determine an average
turntable tare for each velocity. Because of the spread in the bending-
moment data, inaccuracies possibly as large as the tare may exist in the
computed pitching moments on the model.

RESULTS AND DISCUSSION

Measurements on the Basic Configuration

Typical values of the maximum bending moment at the base are pre-
sented in figure 8 for the model with no attachments or modifications.
The maximum bending moment at the base is sufficient to define the stresses
at all points on the model since the strain gages at other stations always
indicated a first-mode moment distribution like that in figure 2, within
the accuracy of the data. Figure 8 shows that the bending moments gener-
ally increased with velocity ,and that the transverse moments were much
larger than the dragwise moments for the basic configuration. The drag-
wise moments in figure 8 are the maximum occurring within one or two
cycles of the maximum transverse fluctuation. The "resultant" shown in
the figure is the vectorial sum of the transverse and dragwise moments
and is little different from the transverse. For this reason most of
the discussion will be concerned with bending moments in the transverse
direction. The Reynolds number scale is shown in its approximate relation
to velocity for all dynamic tests and shows that the Reynolds number was
supercritical (greater than about 500,000) based on either the first- or
second-stage diameter. Points from the repeat test give an idea of data
repeatability with the only change being a reduction of the length of data
sample from about 1 minute to about 30 seconds. The straight-line fairing
between points will be used in succeeding figures and the points will be
eliminated for simplicity.

The agreement between repeat measurements on the basic configuration
was less satisfactory than the case just considered when a greater time
interval and model changes occurred between tests. Figure 9 is a compar-
ison of transverse bending moments from tests made at various times
throughout the investigation. It is apparent that little significance
can be attached to small differences resulting from configuration changes.
At the same time, however, the great improvement resulting from the addi-
tion of a nose spoiler (to be discussed later) is obvious. It was sus-
pected that the bending moments shown in figure 9 might, at times, be
isolated peaks nonrepresentative of the motion. To investigate such a
possibility a statistical analysis was made of several points in the
regions of both good and poor repeatability. Figure 10 shows the number
of transverse bending-moment fluctuations exceeding nominal values for
four test velocities plotted on normal-probability graph paper. The data
sample at each velocity contained about 800 cycles. The figure shows

that the peak values are random and that the maximum measured value in all cases is representative of the entire data sample. The poor repeatability is thus not primarily a result of inadequate sampling. It is acknowledged that the label "maximum" is not strictly correct when applied to any of the measured values since the probability of reaching any given stress depends on the length of data sample. However, sufficiently long data samples were obtained to represent almost 20 minutes on the full-scale missile (with little change in the measured maximum to be expected for intervals several times as long). The measured maximums are therefore considered to be the results of most practical interest.

As previously noted, other measurements of the model oscillation were made, and these are compared with the maximum bending-moment data in figure 11 for one of the basic model tests. The close agreement of the trends indicated by the maximum bending moments, the root-mean-square bending moments, and the tip deflections is typical of all tests. The ratio of 3 between root mean square and maximum bending moments is also typical. It should be noted that the tip deflections were derived from the battery-powered tip accelerometer which had an electrical system that was completely isolated from the strain-gage system. Even the base acceleration, although orders of magnitude less than the tip acceleration, had a variation with wind velocity that was similar to the base bending-moment variation. (Movement of the base is attributed to flexing of the tunnel shell.) The pressure fluctuation is that of the pressure difference across the maximum width of the second stage. As mentioned in the Data Reduction section, the analysis of the pressure data is summarized for only one frequency, and the area to which the measured pressures apply is quite limited. Nevertheless, the effect of velocity on pressures is reasonably consistent with that shown by the other measurements. It is concluded that the poor repeatability of the data shown in figure 9 is not a result of instrumentation error. The characteristics of the model motion apparently changed from time to time, possibly as a result of surface conditions of the model or some such unknown. Of the several types of measurements made, the maximum bending moments at the base have been selected as the most useful representation of the model motion.

Transverse Bending Moments

The most surprising result of the tests was the large effect on the transverse bending moments of small modifications to the nose. In figure 12 the maximum transverse bending moments of several configurations are compared. It is seen that spoilers mounted on the nose of the model normal to the air stream produced substantial reductions in the transverse fluctuation. The spoilers on the conical portion of the nose extended 1/2 inch from the surface. The addition of a 1/2-inch rod (representing a probe) had little effect, however. It was reasoned that three-dimensional effects were influencing the flow separation on the cylindrical

part of the second stage. An effort to eliminate this influence was made by attaching an end plate under the nose cap as shown in figure 4(c). The plate extended downstream a distance equal to the diameter of the model at the station of attachment. Figure 13 shows the large reduction in transverse bending moments due to this plate. The figure also shows that a smaller horizontal plate did not produce much of an effect and that a streamwise vertical vane was perhaps adverse to the fluctuation. This latter effect demonstrates that the aerodynamic damping to be gained from such a surface is inconsequential.

The tip effects were further explored by tests of various nose shapes, and the results are shown in figure 14. The extended-nose configuration was the only one showing much improvement over the basic shape. This configuration consisted essentially of the basic shape with an added cylinder having a diameter about 1/3 of the second-stage diameter. The extension was actually accomplished by a change from the original nose in its entirety to one of solid wood construction. To check the effect of the change in mass distribution on the results, a repeat of the basic test was made after the small nose extension had been cut off and the remaining portion was rounded off (this modification gave a negligible mass change). The check test is identified in figure 14, and it is noted that good agreement was obtained with the earlier test.

It appears from the foregoing that three-dimensional effects had a powerful influence on the fluctuating loads. A possibly similar result has been indicated for subcritical Reynolds numbers in reference 5, which notes that an unexpectedly large end effect was observed in the dynamic-pressure measurements on a "two-dimensional" cylinder. To understand the tip effect it would be desirable to know both the amplitude of the pressure fluctuations at various longitudinal stations and the phase relation of the fluctuations at various stations. In the present tests, no information was obtained on the phase relations, but it was determined that nose revisions which reduced the transverse bending moments generally reduced the measured pressure fluctuations at the natural frequency of the model. No values are presented since the scope of the measurements was so limited.

Another effect pursued at some length was that of spoilers mounted on the cylindrical portion of the second stage. In figure 15 are shown the effects of attaching spoilers 1/2 inch high in planes perpendicular to the wind direction (lower three configurations) and 45° from the wind direction (fig. 4(h)). All were effective in reducing the transverse bending moments. Figure 16 shows that a reduction in spoiler height caused a loss in effectiveness at some velocities.

The results in figure 17 show that roughness on the surface of the cylindrical sections increased the transverse bending moments at the lower velocities. The roughness was in some cases carborundum particles blown on the surface after an adhesive had been applied. The particles
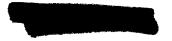
covered approximately 10 percent of the area. Alternatively, garnet paper having the same size particles in a more dense coverage was glued to the model. The results with varying amounts of roughness were remarkably similar. There is also a strong resemblance of the effects of roughness to those of the smallest spoilers in figure 16. Roughness applied to the nose with approximately 50-percent coverage of the area had a comparatively small effect.

The transverse bending moments on the model in the presence of an umbilical tower are compared in figure 18 to the moments for the basic model from a test immediately preceding the tower tests. The moments were greatly reduced when the tower acted as a windscreen for the model in the 0° position. The largest adverse tower effect occurred when the tower was in the 90° position, as shown in figure 18.

Dragwise Bending Moments and Forces

The maximum fluctuation in dragwise bending moment observed throughout each data sample was always less than the maximum transverse bending moment but, when added to the steady (i.e., average) dragwise loads, exceeded the transverse loads on some configurations. The fluctuating and the steady components of the dragwise loads have been separated to show more clearly the various effects of interest. The maximum bending-moment fluctuations in the dragwise direction for several configurations are presented in figure 19. The reduction caused by the tip spoiler is typical of the effects due to other tip modifications which reduced the transverse oscillations. Fluctuations of the dragwise bending moment as high as 40,000 inch-pounds were obtained on other tests of the basic model. This was the largest value observed for any of the configurations. The records of the motions, both wind on and wind off, indicated that very little energy associated with the oscillatory motion was passed back and forth between the dragwise and transverse directions. This was fortunate from the standpoint of interpreting the results, particularly since the structural damping was different in the two directions. It is perhaps worthy of mention that this independence could not be established until all the looseness in the model mounting had been eliminated.

The steady component of the dragwise load was most accurately determined in the static-force tests. The drag coefficients of the basic model are shown in figure 20 for a range of Reynolds numbers from 70,000 to 7,000,000. Drag data from reference 6, which are typical of measurements on two-dimensional cylinders, are shown for comparison. The data for the missile model at low Reynolds numbers are only approximate because of the very low dynamic pressures involved, but they show the usual drag decrease that occurs at the critical Reynolds number. At the higher Reynolds numbers the drag coefficient approached a constant value of approximately 0.5. The effects of various configuration changes on the steady drag are

CONFIDENTIAL
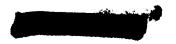
shown in figure 21. It is interesting to note that the end plate, which was so effective in reducing the transverse loads, decreased the steady drag component also. The tip spoiler had a similar but smaller effect. The center of pressure of the steady drag computed from the steady overturning moment and drag is shown in figure 22. At the highest Reynolds numbers the center of pressure of the steady drag fell approximately on the centroid of frontal area. In terms of moment, the steady drag loads were approximately the same as the dragwise moments presented in figure 8, where the fluctuation component was generally small. It should be reiterated that the evaluation of model-support tares in the static tests involved approximations which leave a possible inaccuracy in the over-all level of the centers of pressure of 7 or 8 inches.

CONCLUSIONS

Wind-tunnel tests at Reynolds numbers up to 7 million per foot have been performed on a 1/10-scale model of the Titan missile in launching position. The following results were obtained:

1. For some test configurations, the transverse loads induced by the wind were much larger than the dragwise loads.

2. At all test velocities, the measured pressure fluctuations and the amplitude of the model response were random in nature.

3. Certain small additions or modifications to the nose reduced the amplitude of the transverse fluctuations.

4. Flow spoilers on the cylindrical sections near the nose were also effective in reducing the transverse fluctuations.

5. A rough model surface or an adjacent structure increased the fluctuations at some speeds.

6. At the highest Reynolds numbers the average drag coefficient of the basic model was about 0.5 and the center of pressure was approximately on the centroid of frontal area.

Ames Research Center
    National Aeronautics and Space Administration
        Moffett Field, Calif., July 28, 1959

DECLASSIFIED CONFIDENTIAL 13

REFERENCES

1. Ozker, M. S., and Smith, J. O.: Factors Influencing the Dynamic Behavior of Tall Stacks Under the Action of Wind. Trans. ASME, vol. 78, no. 6, (Aug. 1956) pp. 1381-1391.

2. Fung, Y. C.: Fluctuating Lift and Drag Acting on a Cylinder in a Flow at Supercritical Reynolds Numbers. Space Tech. Lab. Rep. No. EM 8-5, 1958.

3. Fung, Y. C.: The Fluctuating Lift Force Acting on a Cylinder Subjected to Forced Oscillations Perpendicular to a Flow at High Reynolds Numbers. Space Tech. Lab. Rep. No. EM 8-19, 1958.

4. Herriot, John G.: Blockage Corrections for Three-Dimensional-Flow Closed-Throat Wind Tunnels, With Consideration of the Effect of Compressibility. NACA Rep. 995, 1950. (Supersedes NACA RM A7B28)

5. Gerrard, J. H.: Measurements of the Fluctuating Pressure on the Surface of a Circular Cylinder. Part 1. Cylinder of 1-Inch Diameter. British ARC Rep. 19,844, 1958.

6. Wieselsberger, Carl: New Data on the Laws of Fluid Resistance. NACA TN 84, 1922.
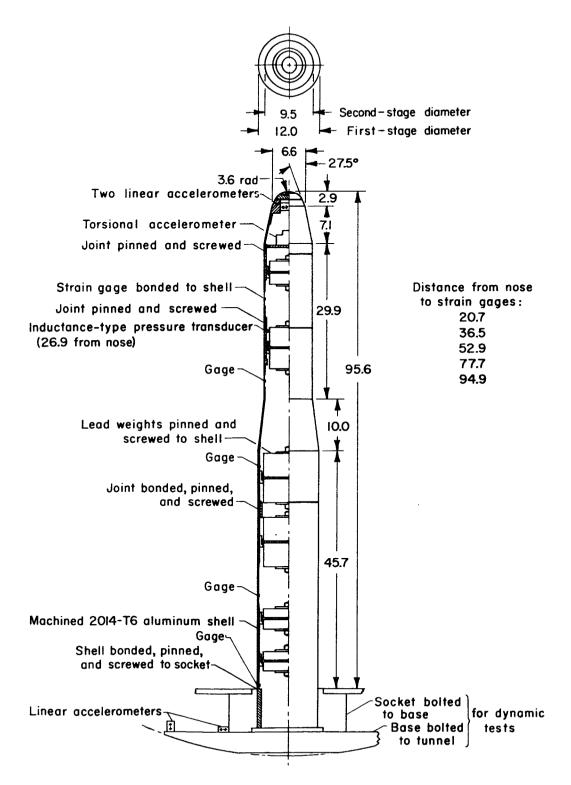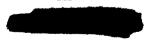
Figure 1.- Dimensions and details of the model. Lineal dimensions in inches.
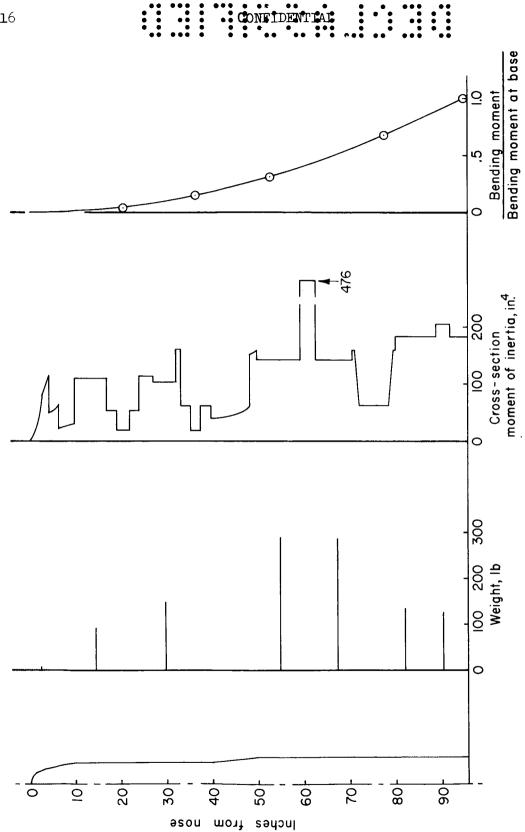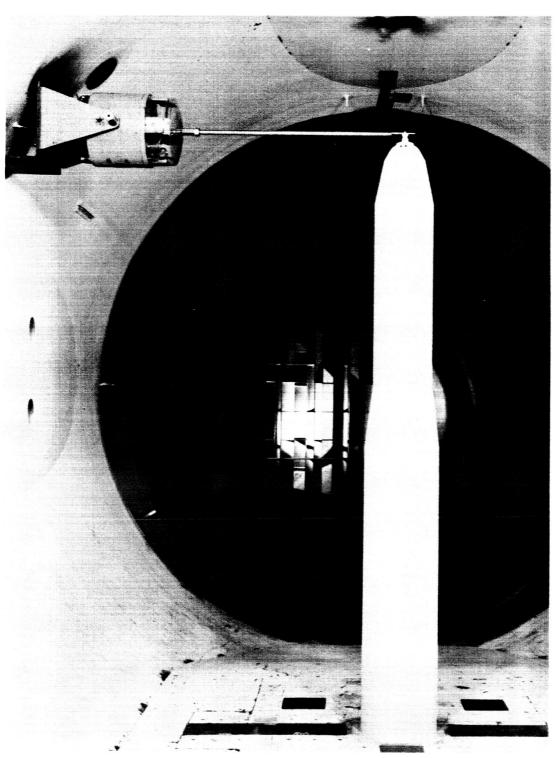
Figure 2.- Distribution of weight, cross-section moment of inertia, and measured first-mode bending moments of the model.

A-173

A-24156

Figure 3.- The model installed in the wind tunnel. Shaker, shown
connected to tip, installed for wind-off tests only.

(a) Tip spoiler 1 inch high.

(b) Horizontal plate extending 1/2 inch.

(c) Horizontal "end plate" extending 5.4 inches downstream.

(d) Streamwise tip vane 6×6 inches, 12 percent thick.

(e) Blunt nose.

(f) Conical nose.

(g) Nose extended 7 inches with 3-1/4-inch cylinder.

(h) Side spoilers extending 1/2 inch.
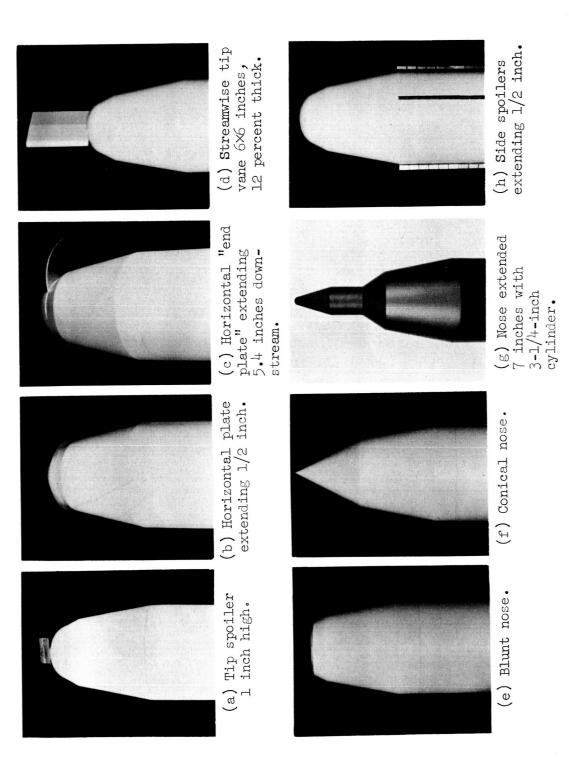
Figure 4.- Model nose portion with some of the additions and modifications tested. Upstream direction to left and rear of camera.

A-23891
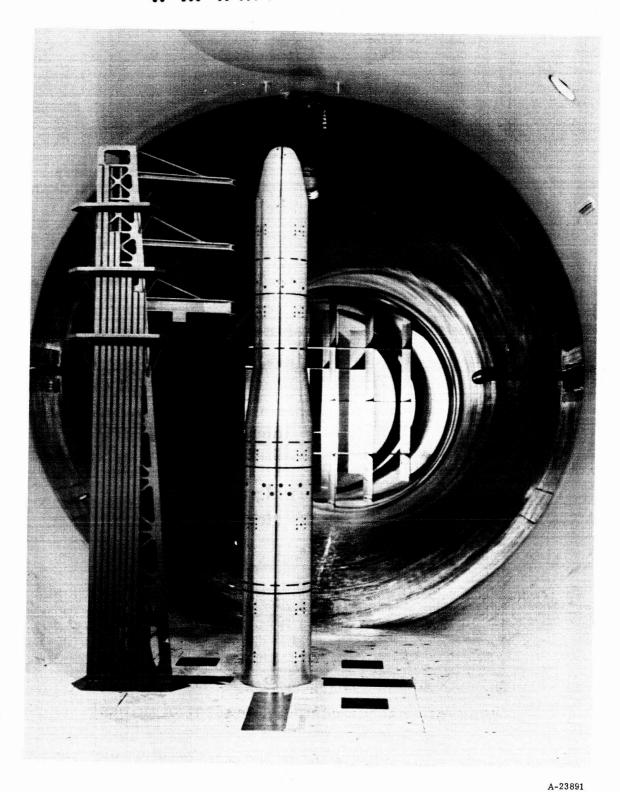
Figure 5.- Umbilical tower installed in the 90° position.
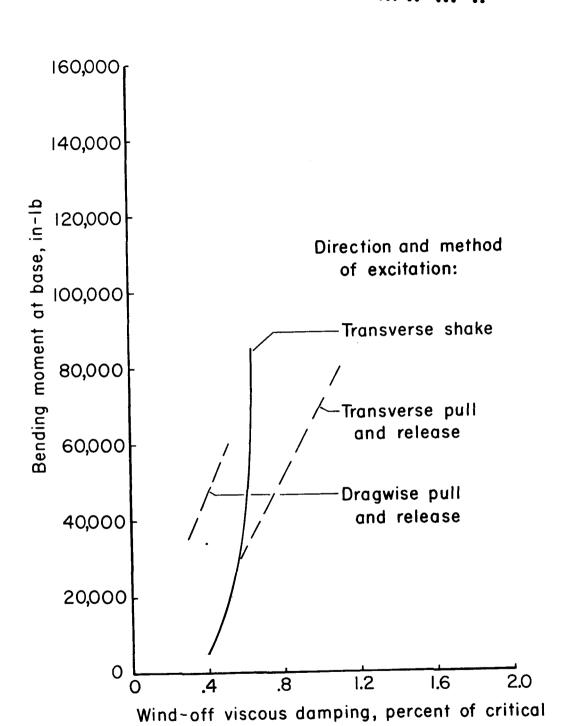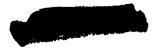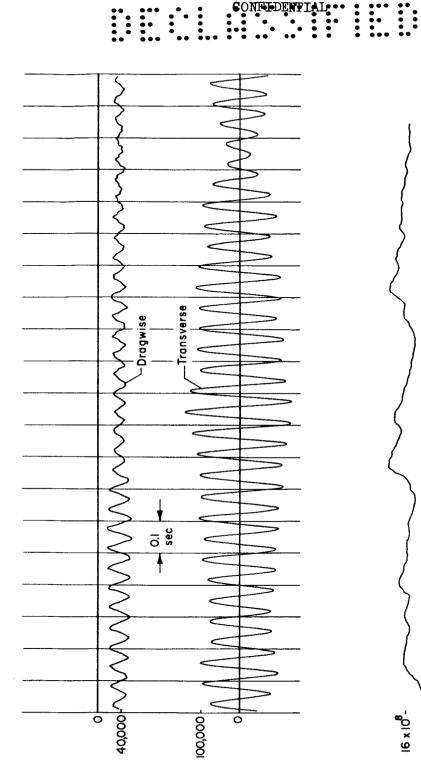
Figure 6.- The structural damping of the model measured with the
wind off.

Dragwise

Transverse

0.1
sec

O

40,000

100,000

O

Bending moment at base, in-lb

Time

5 sec

16×10^8

O

Mean-squared transverse bending
moment at base, $(in-lb)^2$
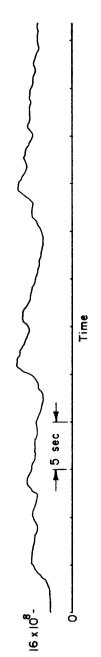
Figure 7.- Samples of the strain-gage outputs and the mean-square meter output.
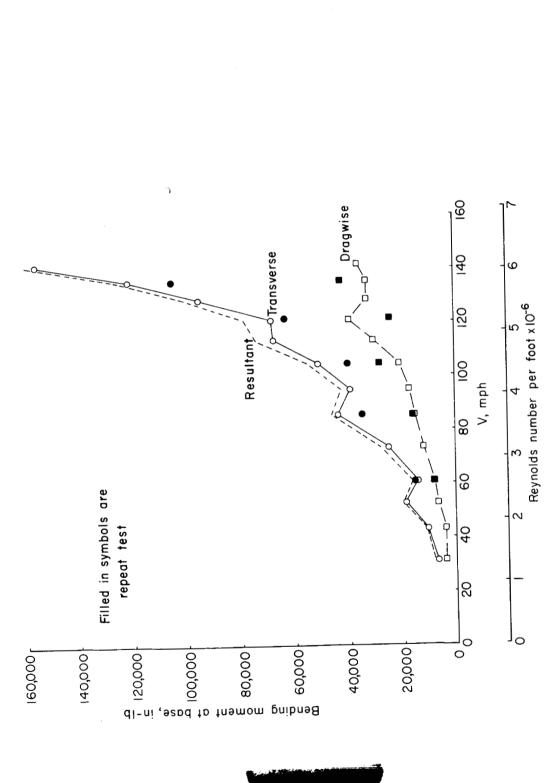
Figure 8.- Typical maximum bending moments for the basic model. Bending moments measured at time of maximum transverse deflection.

CONFIDENTIAL
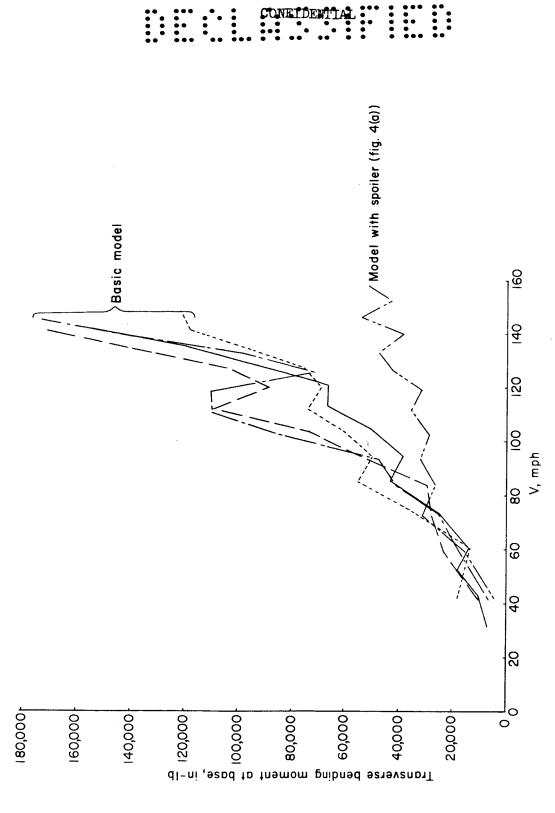
Figure 9.- Comparison of maximum bending moments from tests performed at various times throughout the investigation.
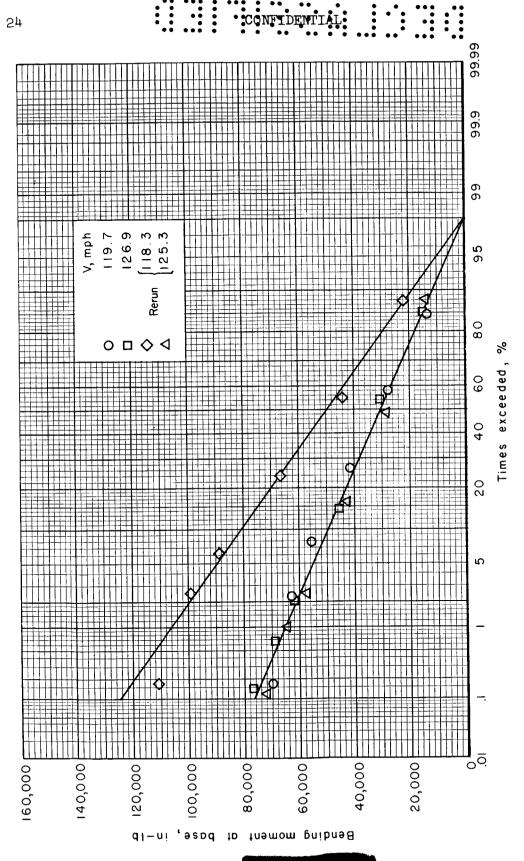
Figure 10.- An analysis of four data samples showing the number of times that peak bending moments in a transverse direction exceeded nominal values. Results plotted on normal probability graph paper.
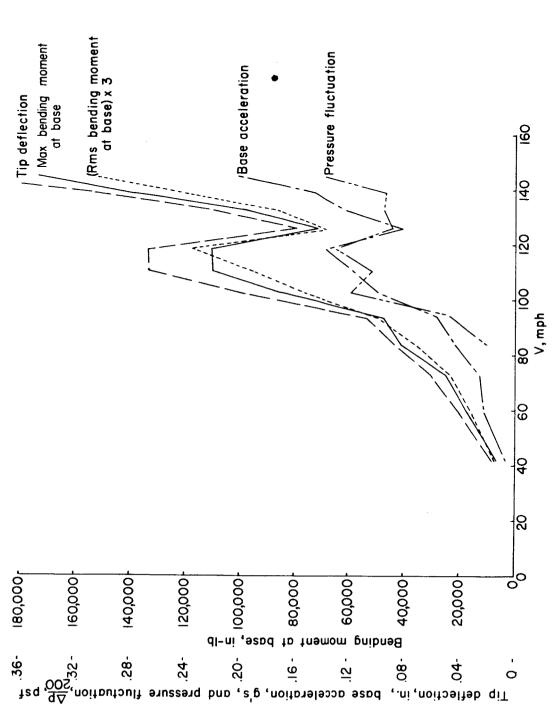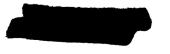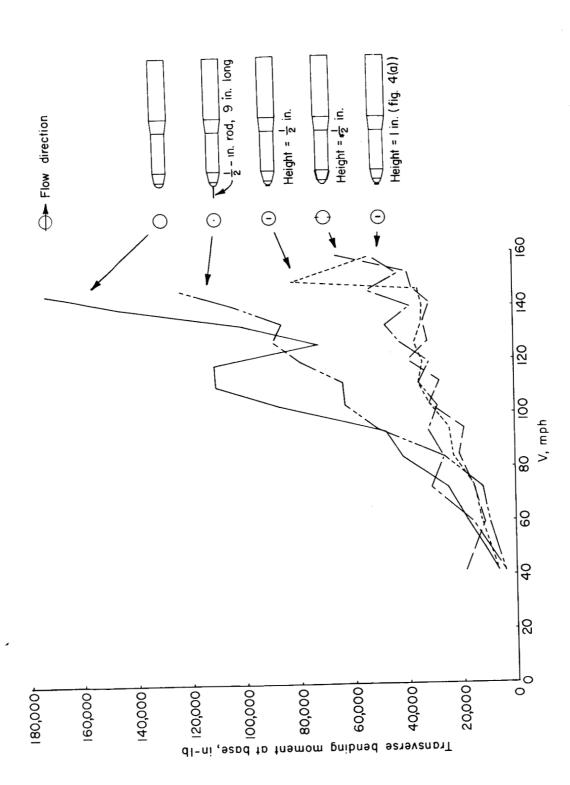
Figure 11.- A comparison of various measurements associated with the transverse oscillations of the model.
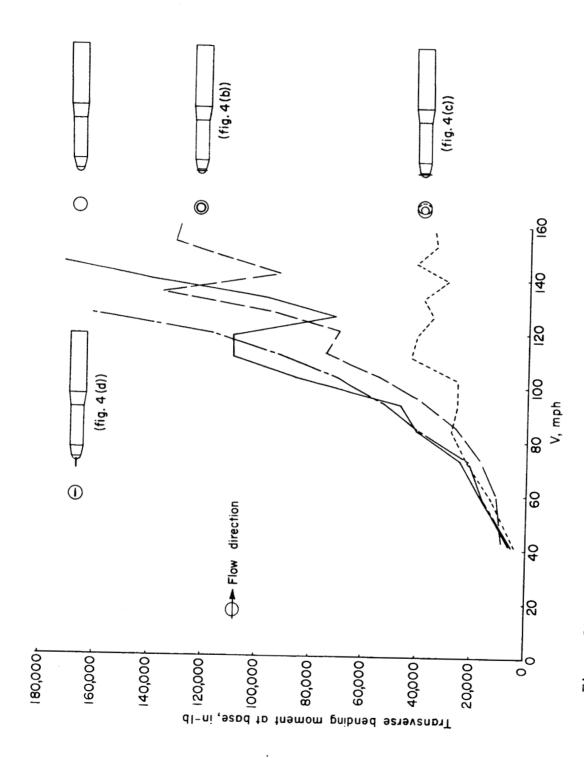
Figure 12.- The effects of protuberances at the nose of the model on the maximum transverse bending moments.

A-173

Figure 13.- The effects of flow dividers on the maximum transverse bending moments.
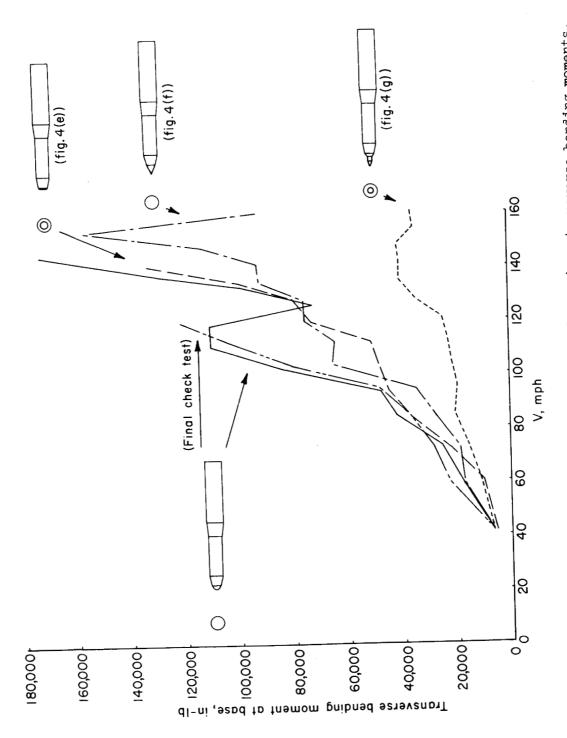
Figure 14.- The effects of nose shape on the maximum transverse bending moments.

CONFIDENTIAL
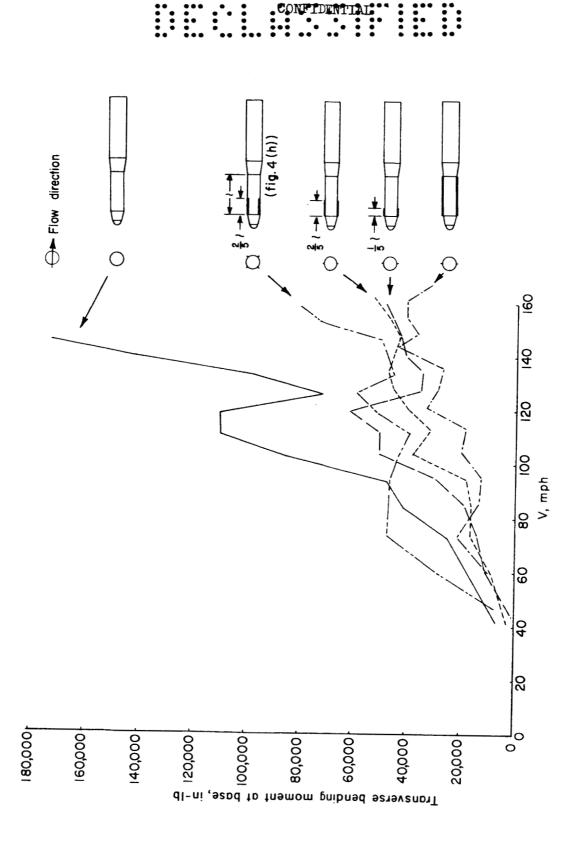
Figure 15.- The effects of spoiler location on the maximum transverse bending moments. Spoilers extend 1/2 inch from surface.
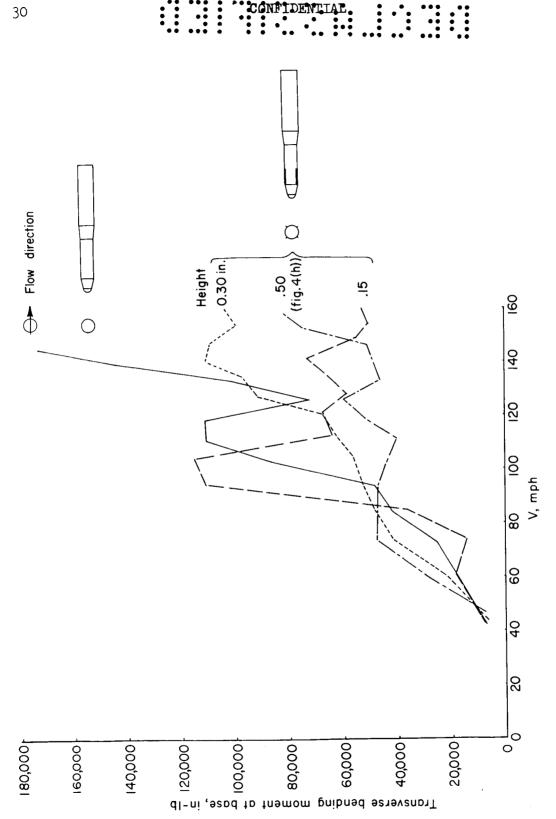
Figure 16.- The effects of spoiler height on the maximum transverse bending moments. Spoilers extend 2/5 l.
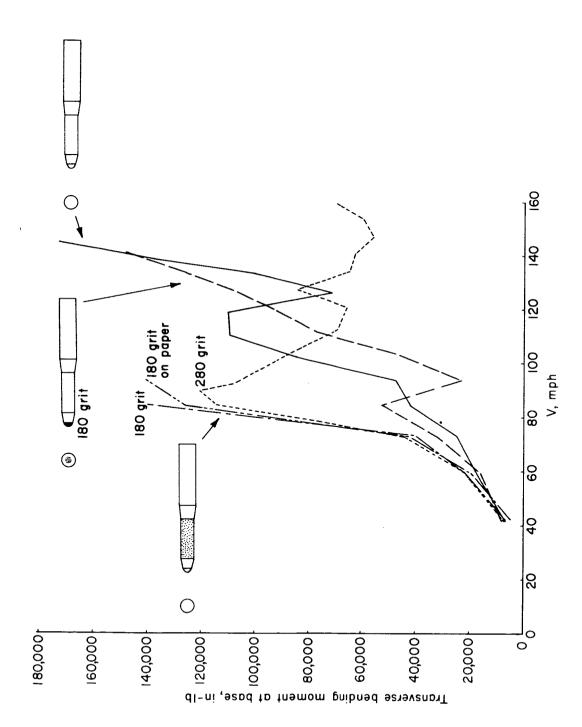
Figure 17.- The effects of surface roughness on the maximum transverse bending moments.
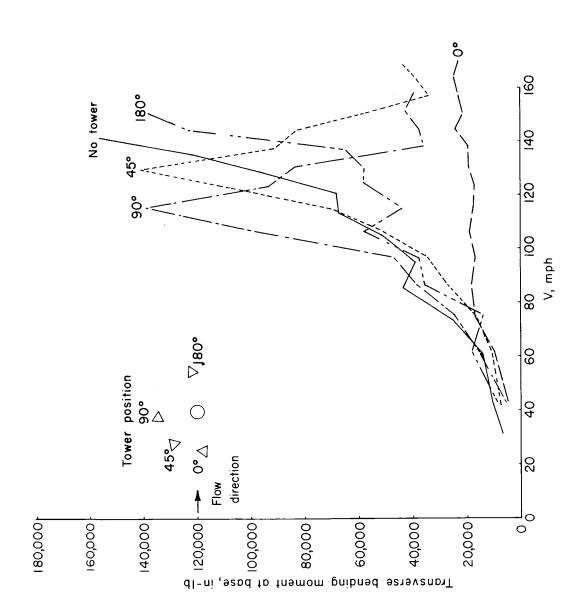
Figure 18.- The effects of the umbilical tower on the maximum transverse bending moments.
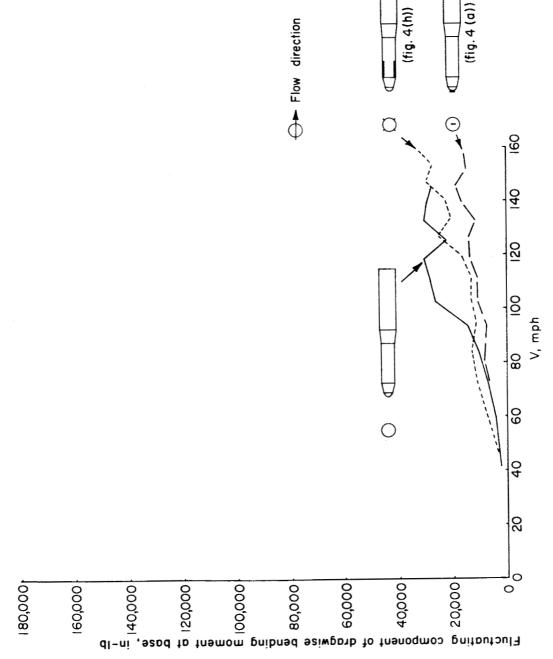
Figure 19.– The effects of model modifications on the maximum dragwise bending-moment fluctuations (one-half of difference between peak values).
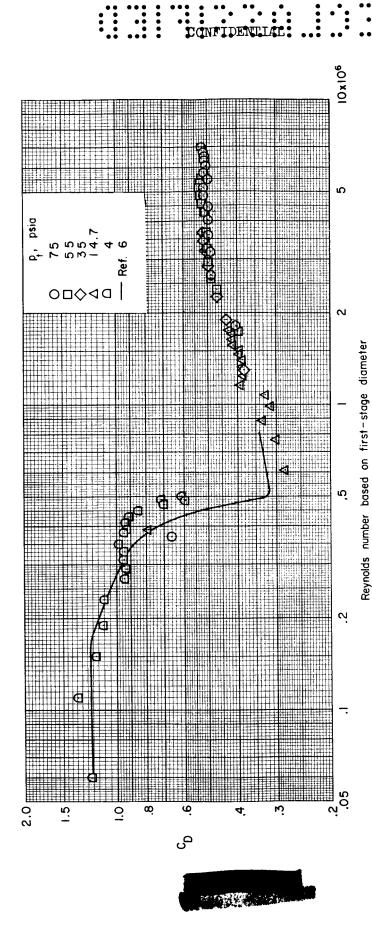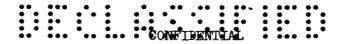
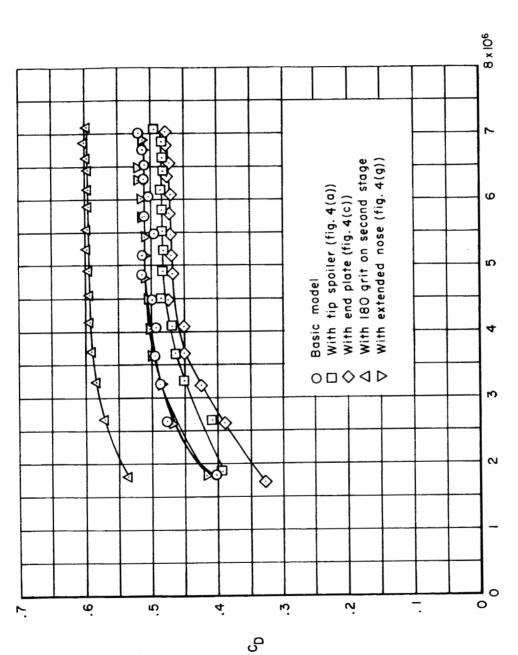Figure 20.- The steady-drag characteristics of the basic model compared with two-dimensional-cylinder data.
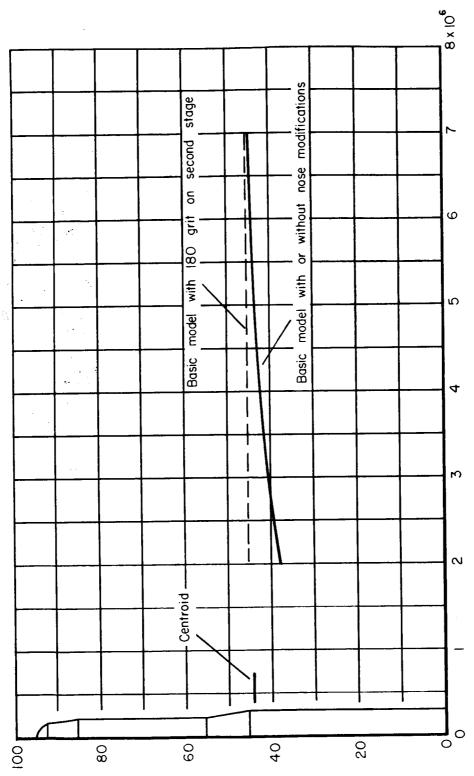
Figure 21.- The effects of model modifications on the steady-drag characteristics.

Figure 22.- The location of the center of pressure of the steady drag.